Massive Volcanism May Have Foreshortened the Marinoan Snowball Earth

Zhongwu Lan, Magdalena Huyskens, Guillaume Le Hir, Ross Mitchell, Qing-zhu Yin, Gangyang Zhang, Xian-hua Li

Massive Volcanism May Have Foreshortened the Marinoan Snowball Earth

Zhongwu Lan[1,2,3] , Magdalena H. Huyskens[4] , Guillaume Le Hir[5] , Ross N. Mitchell[1,6] , Qing-Zhu Yin[4] , Gangyang Zhang[7] , and Xian-Hua Li[1,6]

[1]State Key Laboratory of Lithospheric Evolution, Institute of Geology and Geophysics, Chinese Academy of Sciences, Beijing, China, [2]State Key Laboratory of Palaeobiology and Stratigraphy, Nanjing Institute of Geology and Palaeontology, Chinese Academy of Sciences, Nanjing, China, [3]State Key Laboratory of Geological Processes and Mineral Resources, China University of Geosciences, Wuhan, China, [4]Department of Earth and Planetary Sciences, University of California, Davis, Davis, CA, USA, [5]Institut de Physique du Globe de Paris, Université Paris, Paris, France, [6]College of Earth and Planetary Sciences, University of Chinese Academy of Sciences, Beijing, China, [7]College of Earth Sciences, Chengdu University of Technology, Chengdu, China

Abstract The Cryogenian Period (717–635 Ma) experienced two low-latitude "snowball Earth" glaciations, the Sturtian and the Marinoan of contrasting 57 and <16 Myr durations, respectively. A lack of reliable age controls on extensional tectonics and associated magmatic rocks during the Marinoan has hampered an understanding of the deglaciation. Furthermore, although deglaciation is generally assumed to have occurred once ongoing magmatism accumulated enough atmospheric CO_2, as suggested by cap carbonates, specific geologic evidence linking volcanic events with deglaciation are lacking. Here, we present high-precision zircon geochronology with chemical abrasion-isotope-dilution isotope ratio mass spectrometry that indicates an extensive and thick sequence of rift-related magmatic rocks in South Qinling, Central China, erupted 2–6 Myr before the termination of the Marinoan. Climate modeling proposes a scenario explaining why the Marinoan was the shorter snowball and how volcanism may have driven the deglaciation.

Plain Language Summary Volcanic CO_2 and dust emissions have been regarded as the major driver for Marinoan deglaciation. Most of CO_2 outgassing is associated with seafloor spreading and subduction (arc magmatism), which are ongoing processes on geological timescales. To drastically increase CO_2 emissions, there must have been many active rift zones during Marinoan glaciation. We provide age constraints on a previously little-known major Marinoan rift-related volcanic suite in South Qinling, which reveals volcanic activity lasting 4 Myr and ending 2 Myr before the termination of the Marinoan snowball Earth. Climate modeling provides constraints for the ice-age duration deduced from the geological setting.

1. Introduction

The Neoproterozoic glaciations were geologically profound events in that they not only changed the chemical and redox conditions of the ancient oceans, but they were also followed by a rapid postglacial diversification of complex eukaryotes eventually culminating in the Cambrian "explosion" of animal life (Erwin et al., 2011; Hoffman et al., 2017). Two Neoproterozoic glaciations have been reported in the Cryogenian Period (ca. 717–635 Ma [Nelson et al., 2020]): the earlier Sturtian and the later Marinoan glaciations (Condon et al., 2005; Hoffman et al., 1998; Zhou et al., 2019). Cryogenian glaciogenic diamictites often interrupt carbonate sequences (Hoffman et al., 1998; Zhou et al., 2019) and occur at low paleolatitudes, providing a lithologic and paleomagnetic basis for the snowball Earth hypothesis (Kirschvink, 1992). Such Cryogenian occurrences are now known worldwide and have been established as synchronous (Nelson et al., 2020; Zhou et al., 2019).

The snowball Earth hypothesis assumes that a runaway ice-albedo feedback induced Earth's surface temperatures to plummet and prompted polar ice sheets to quickly conceal the tropical oceans (Hoffman & Schrag, 2002). During a snowball, however, tectonics and magmatic outgassing would have continued and eventually accumulated a large amount of atmospheric CO_2, creating an intense greenhouse condition to counteract the ice-albedo effect (Kirschvink, 1992; Tamburello et al., 2018). A series of model simulations and geochemical proxy calculations suggest that despite CO_2 sinks by means of seafloor weathering, a threshold CO_2 level can still be reached for CO_2 radiative forcing to have initiated deglaciation (H. Bao et al., 2009; Le Hir, Ramstein, et al., 2008; Pierrehumbert et al., 2011). Once started, deglaciation would drive ice lines to rapidly retreat and end up in the ice-free

Methodology: Magdalena H. Huyskens, Guillaume Le Hir, Qing-Zhu Yin
Project Administration: Zhongwu Lan, Qing-Zhu Yin, Xian-Hua Li
Resources: Gangyang Zhang
Software: Magdalena H. Huyskens, Guillaume Le Hir, Qing-Zhu Yin
Supervision: Zhongwu Lan, Qing-Zhu Yin, Xian-Hua Li
Validation: Zhongwu Lan, Magdalena H. Huyskens, Guillaume Le Hir, Ross N. Mitchell, Xian-Hua Li
Visualization: Zhongwu Lan, Magdalena H. Huyskens, Guillaume Le Hir, Ross N. Mitchell
Writing – original draft: Zhongwu Lan, Magdalena H. Huyskens, Guillaume Le Hir, Ross N. Mitchell, Qing-Zhu Yin, Gangyang Zhang
Writing – review & editing: Zhongwu Lan, Magdalena H. Huyskens, Guillaume Le Hir, Ross N. Mitchell, Qing-Zhu Yin, Gangyang Zhang

state, where such fast glacial retreat and rapidly warming surface temperatures allowed for the precipitation of the diagnostic "cap" carbonates sitting on top of Cryogenian glacial deposits in <1 Myr (Zhou et al., 2019). Insofar as the magmatism-related outgassing mechanism for deglaciation is generally accepted, it remains elusive to explain why the Sturtian and Marinoan glaciations have such different durations. The former has a duration of 57 Myr (716–659 Ma), whereas the latter has a duration of <16 Myr (<651–635 Ma; Nelson et al., 2020; Zhou et al., 2019). Given the potential for dirty snow and the accumulation of dust on ice (de Vrese et al., 2021; Pierre-humbert, 2005), the snowball termination could have resulted from a combination of decreasing surface albedo and build-up of CO_2, both related to massive volcanic events.

While the final stage of the Marinoan deglaciation is well-constrained at ca. 635 Ma based on radiometric dates from volcanic ash layers bracketing postglacial cap carbonates, this age alone is not adequate to quantify the amount of time it took to accumulate abnormally high atmospheric CO_2 concentrations, which likely took several million years (Hoffman et al., 1998, 2017). Geological and geochronological evidence has increasingly demonstrated the occurrence of ca. 650–635 Ma rift-related magmatism in the South Qinling terrane of the South China Craton, as well as in the Tarim, Siberia, and Congo cratons (Deng et al., 2016; Prave et al., 2016; Vernikovsky et al., 1999; M. X. Wang, Wang, & Zhao, 2013; Xue et al., 2011; Yarmolyuk et al., 2005; Zhu et al., 2008, 2014, 2015). However, with the exception of one study (Prave et al., 2016), most of these radiometric dates are imprecise. Nonetheless, the ages are within analytical uncertainty of each other, with the oldest ages centering around 640 Ma, and possibly suggest an initial period of pronounced magmatism during the Marinoan glaciation.

In this work, we document ca. 640 Ma rift-related magmatic rocks from South Qinling, Central China, occurring stratigraphically below the cap carbonates. This critical discovery provides a direct link between evidence of rift-related magmatism and the termination of the Marinoan glaciation. The consequences of the South Qinling rift system are explored using climate modeling with the purpose to quantify the foreshortening of the Marinoan glaciation compared to its Sturtian counterpart.

2. Geological Setting and Sampling

The South China Craton are formed by the merging of the Yangtze and Cathaysia blocks (Figure S1 in Supporting Information S1; Li et al., 2002). Subsequent rifting is recorded in the Nanhua basin containing well-preserved Neoproterozoic (850–541 Ma) volcano-sedimentary strata (J. Wang & Li, 2003). The suite of interbedded sedimentary and volcanic rocks are well exposed in the Hunan-Guizhou-Guangxi regions and hosts information related to the evolution of supercontinent Rodinia and the snowball Earth glaciations (Lan et al., 2014, 2015). The slope-basinal facies are well exposed with a maximum thickness in the southeast of the South China Craton and the platform facies to the northwest are poorly exposed (Zhou et al., 2019). In the northern margin of the Yangtze block, Cryogenian successions are incomplete, where the Nantuo Formation is unconformably underlain by the Liantuo Formation. The Liantuo Formation is Tonian (ca. 780–720 Ma) and correlates with the middle-late Tonian successions in the Hunan-Guizhou-Guangxi area (Lan, Li, Zhang, & Li, 2015; Lan, Li, Zhu, et al., 2015), whereas the Nantuo Formation ranges from ca. 650–635 Ma and thus correlates with the Marinoan glaciation (X. Bao et al., 2018; Condon et al., 2005; Zhou et al., 2019).

The South Qinling terrane was originally connected to the northern Yangtze block during the Neoproterozoic (Figure S1 in Supporting Information S1; Dong et al., 2016; R. Zhang et al., 2016). Volcanic and volcanoclastic rocks of more than 2 km in thickness are a typical lithological assemblage within the South Qinling terrane that are represented by the Wudang and Yaolinghe groups and are overlain by the Ediacaran Doushantuo Formation. Such abundant volcanism occurred in a continental rift basin associated with the subsequent separation of South Qinling from the Yangtze block (Ling et al., 2010; Zhu et al., 2008, 2014). Recent zircon U-Pb geochronology constrains the depositional ages of the Wudang and Yaolinghe groups in the range of 780–720 Ma and ca. 650–636 Ma, respectively (Cai et al., 2007; Deng et al., 2016; Ling et al., 2008; M. X. Wang, Wang, & Zhao, 2013; Zhu et al., 2014, 2015). Synchronous, cogenetic mafic-ultramafic intrusions in the Wudang-Suizhou-Zaoyang areas represent the exposed plumbing system of the alkali volcanism in the Wudang area (L. J. Wang, Griffin, et al., 2013; M. Wang, Wang, & Sun, 2013; M. X. Wang, Wang, & Zhao, 2013; Wang et al., 2016; Xue et al., 2011; Zhu et al., 2015). On the basis of these age constraints, the Wudang and Yaolinghe groups are coeval with the Liantuo and Nantuo formations, respectively (Figure 1). Both the Yaolinghe Group and the Nantuo
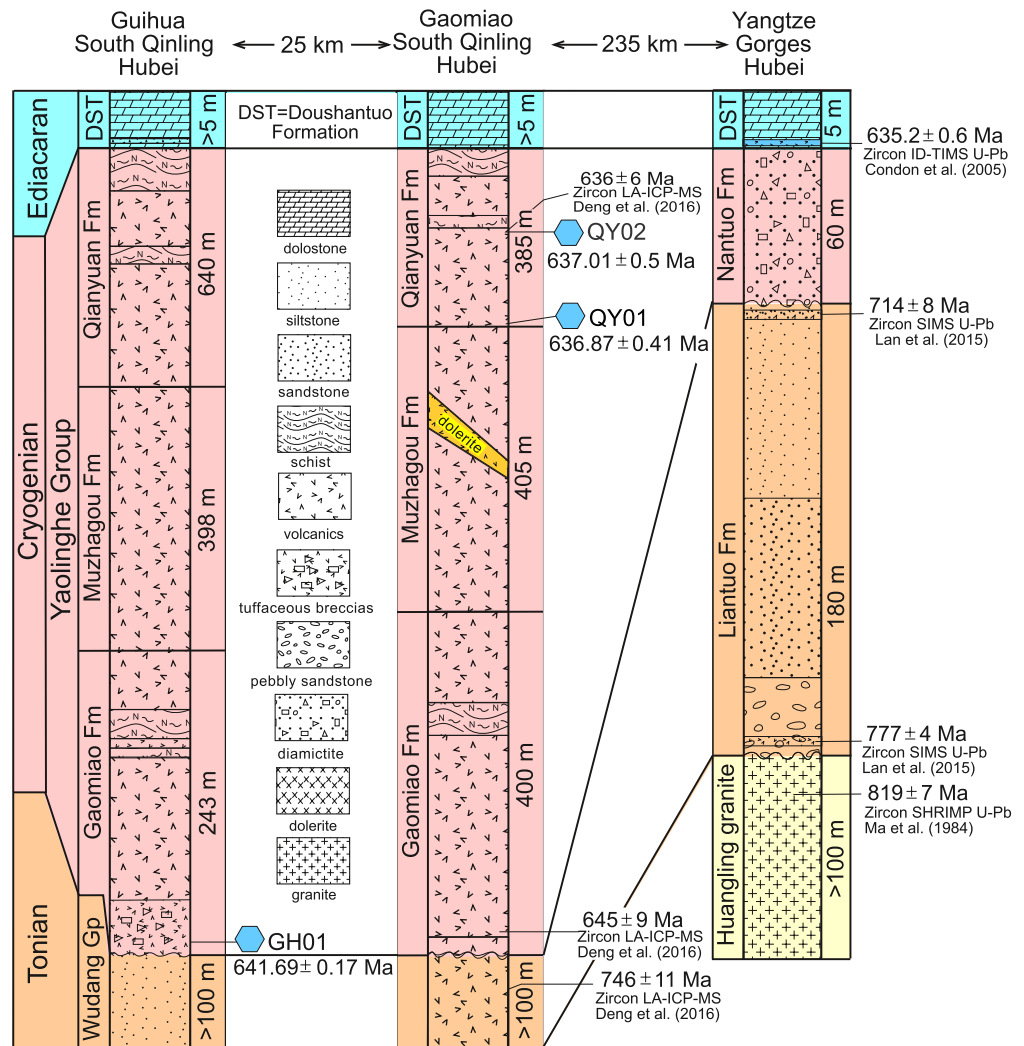
Figure 1. Lithostratigraphy of the Guihua and Gaomiao sections and sampling horizons. The Wudang and Yaolinghe groups in the South Qinling terrane correlate with the Liantuo and Nantuo formations, respectively, from the northern margin of the Yangtze block. Early Cryogenian and interglacial (720–650 Ma) sedimentary successions are absent due to uplift and erosion (e.g., Mitchell et al., 2019). Blue hexagons mark the sampling horizons, with sample names and zircon dates. Fm–formation. Gp–group.

Formation underlie the Doushantuo Formation (L. J. Wang, Griffin, et al., 2013; M. Wang, Wang, & Sun, 2013; M. X. Wang, Wang, & Zhao, 2013), suggesting the synchronous deposition of the Neoproterozoic successions within the South Qinling terrane and the northern margin of the Yangtze block. In this study, a total of 22 volcanic rocks/tuffs were collected from the Yaolinghe Group for geochronological and geochemical studies. Details about the field outcrops and petrography of the samples are provided in the Supporting Information.

3. Results

Zircon CA-ID-IRMS U-Pb dating was conducted using a Triton Plus TIMS and a Neptune Plus. Whole-rock major and trace element geochemical analyses were conducted using an X-ray fluorescence spectrometer (ME-XRF26d) and an Agilent 7500a ICP-MS. Whole rock Nd isotopic analysis was conducted using a Triton Plus multi-collector TIMS. Climate modeling was conducted using a climate-geochemical model (GEOCLIM; Donnadieu et al., 2006). Detailed analytical methods are described in the Supporting Information.
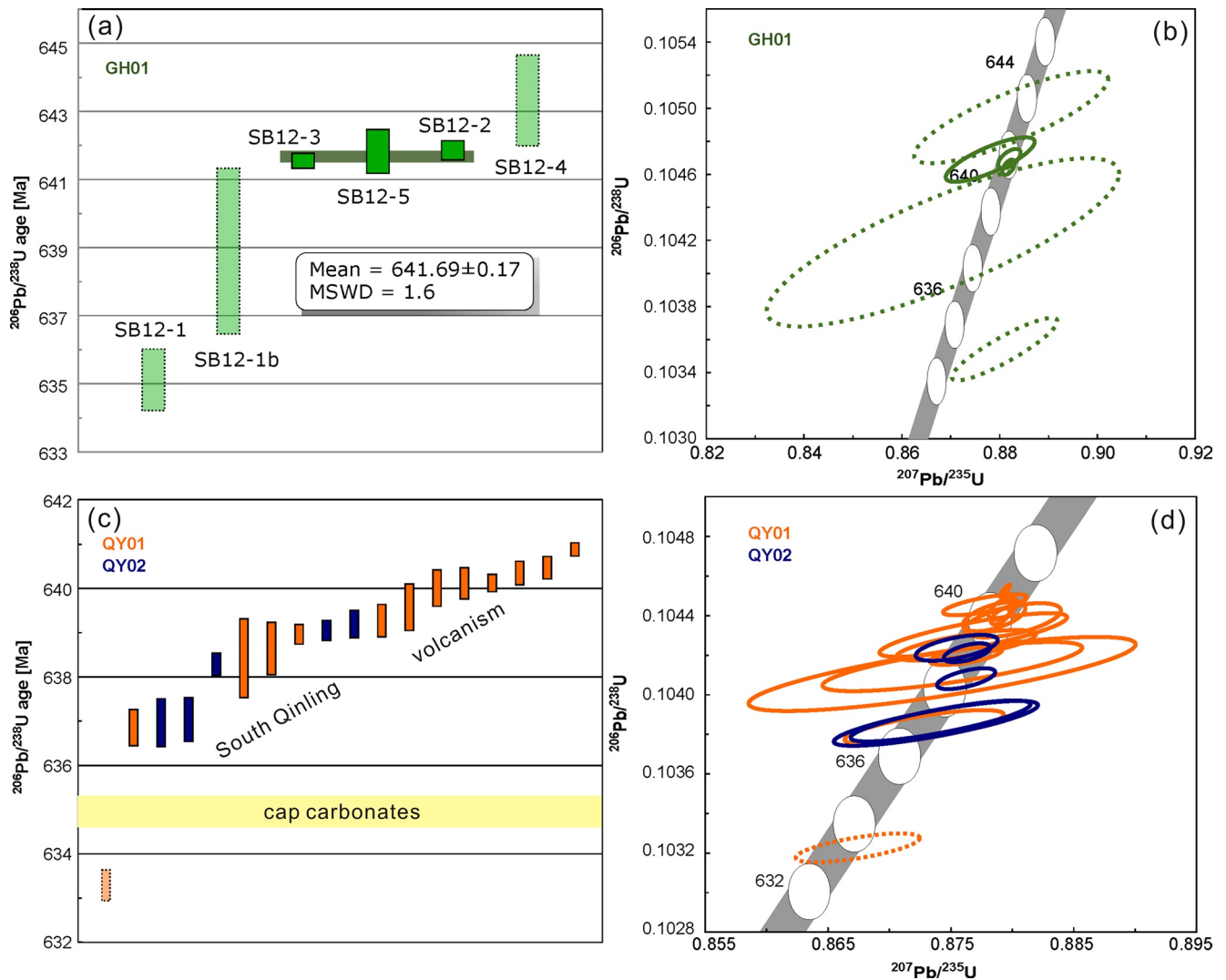
Figure 2. Zircon chemical abrasion-isotope-dilution isotope ratio mass spectrometry U-Pb ages. (a) U-Pb ages from tuffaceous breccia sample GH01, also shown as a Concordia diagram in (b). After rejecting two dates from one split grain due to Pb loss (dotted outline) and one date due to inheritance (dotted outline), an average of ca. 641 Ma is interpreted as the depositional age of basal Yaolinghe tuffaceous breccias. (c) U-Pb ages from rhyolite samples QY01 and QY02, also shown as a Concordia diagram in (d). After rejecting one date due to Pb loss (dotted outline), an average of ca. 637 Ma is interpreted as the eruption age of Yaolinghe bimodal volcanic rocks, while the older dates are interpreted to be antecrysts from earlier magmatic cycles. Sample QY02 was collected from near the top of the rhyolite succession, while QY01 comes from near the bottom (Figure 1). Cap carbonates in South China are precisely dated with U-Pb ages on intercalating ash layers (Condon et al., 2005; Zhou et al., 2019). Note that Yaolinghe volcanism directly precedes the deglacial cap carbonates.

3.1. CA-ID-IRMS U-Pb Geochronology

Results for zircon CA-ID-IRMS U-Pb geochronology are presented in Table S1. Those samples include GH01 (basal tuffaceous breccias) and QY01 and QY02 (basal and top rhyolites, respectively) of the South Qinling volcano-stratigraphic sequence (Figure 1). Overall, zircons from the three samples are very similar in appearance in plain light photomicrographs (Figure S12 in Supporting Information S1). Most of the grains are short prismatic and exhibit oscillatory zoning, although some elongated prismatic grains are present. They have lengths of 50–300 μm and widths of 25–200 μm, with aspect ratios of 1.5–3. GH01 yields a weighted mean age of 641.69 ± 0.17/0.26/1.37 Ma (MSWD = 1.6, $n = 3$, 2σ analytical uncertainty/analytical and tracer calibration uncertainty/analytical and tracer calibration uncertainty including decay constant uncertainty (Villa et al., 2016; Figure 2). The rhyolite samples QY01 and QY02 have $^{206}Pb/^{238}U$ zircon ages between ~641 and ~637 Ma, with the youngest grain of QY01 at 636.87 ± 0.41 Ma, which is interpreted as the closest approximation of the eruption age of the rhyolite. The presence of zircons spanning ~4 Myr indicates prolonged magmatic activity.

Our new CA-ID-IRMS ages of 637–641 Ma from the Yaolinghe Group represent the timing of major phases of volcanic activity around the Wudang rift zone. Previously, the Yaolinghe volcanic rocks were repeatedly dated using SIMS/LA-ICP-MS and produced controversial ages ranging from 685 ± 5 Ma to 636 ± 6 Ma (Deng et al., 2016; Ling et al., 2008; Zhu et al., 2015). Considering inheritance of zircon grains in mafic rocks and large analytical uncertainties, these previous SIMS/LA-ICP-MS radiometric ages are not accurate. Magmatism from ca. 643–635 Ma also occurred in the Tarim, Siberia, and Congo cratons (Prave et al., 2016; Vernikovsky et al., 1999; Yarmolyuk et al., 2005; Zhu et al., 2008). Within uncertainties, these magmatic events are all synchronous with end-Marinoan magmatism in South Qinling and the northern margin of the Yangtze block (L. J. Wang, Griffin, et al., 2013; M. Wang, Wang, & Sun, 2013; M. X. Wang, Wang, & Zhao, 2013).

3.2. Modeling Atmospheric CO_2 Evolution and Snowball Duration

The consequences of the South Qinling rift system have been explored using climate-ice-sheet-carbon modeling. We simulated the pCO_2 evolution by including two major constraints: (a) the duration of snowball Earth, which is 57 Myr for the Sturtian (Condon et al., 2005; Hoffman et al., 1998; Zhou et al., 2019) in comparison to <16 Myr for the Marinoan (Nelson et al., 2020) and (b) the continental ice sheet response to orbital forcing as a function of CO_2 levels (Benn et al., 2015) to compute the weathering efficiency and the coverage of land ice (Supporting Information). Our simulations reveal that, despite the presence of a massive ice sheet (170 millions of km^3; Figure S10 in Supporting Information S1), the meltwater flux remains too limited to counteract the sluggish hydrological cycle (Abbot et al., 2012). As a consequence, weathering fluxes range from 4 to 2 orders of magnitude below their modern values (Figure S13 in Supporting Information S1) as silicate weathering appears to be insensitive to the load of atmospheric CO_2 due to cold surficial conditions. This strong feature of the snowball Earth motivated us to apply a broad range of degassing rates and the changing of the carbon source and processes associated with volcanism to be considered as the most likely assumption to elucidate the ice-age duration.

Before quantifying South Qinling magmatism, we first consider a case where degassing is solely driven by a tectonic setting. As there is no direct proxy for the degassing rate of the solid Earth, aerial degassing rates are derived from subduction zones (Mills et al., 2017) by considering a large range of possibilities from the modern value to the weakest case (38% of the modern value, "deg0.38"; Supporting Information). Our simulations reveal expected deglaciation thresholds associated with a long-lived snowball Earth (>57 Myr) that is supposed to represent the Sturtian glaciation. According to our simulations, a snowball Earth lasting more than 57 Myr seems to be incompatible with a degassing rate as intense as today (Figure 3a). By assuming weaker degassing rates, deglaciation thresholds ($pCO_{2(57 \text{ Myr})}$) range from 0.09 bar (deg0.38) to 0.26 bar (deg0.8) and exhibit a nonlinear function with the degassing rate (Figure 3a). The logarithmic accumulation rate of CO_2 is a direct response to seawater acidification that enhances seafloor weathering (Le Hir et al., 2008a), whereas the nonlinearity is ascribed to the ratio between carbon consumption via seafloor weathering and carbon emission via magmatic degassing. For present-day conditions, seafloor weathering shows a small flux (1.8×10^{12} molC/yr or ~0.08 Gt CO_2/yr) compared to modern degassing (6.8×10^{12} molC/yr or ~0.3 Gt CO_2/yr), with a ratio reaching 3.8. With respect to the background degassing assumption for the Cryogenian, this ratio varies from 1.4 to 3 prior to acidification. As such, a moderate amplification of carbon consumption by seafloor weathering related to a more acidic snowball ocean, is sufficient for balancing the inorganic carbon cycle. Seafloor weathering can be ignored by assuming zero air-sea gas exchange. In this specific scenario, snowball length can be drastically shortened, which would prompt all the emitted CO_2 (~0.24 Gt CO_2/yr for deg0.8) to be stored in the atmosphere instead of the ocean.

To address the issue of foreshortening the Marinoan glaciation, we consider fluctuations of the carbon source assuming that the CO_2 deglacial Sturtian limit can be also applied to the Marinoan. To test this hypothesis, we re-conducted simulations by adding a continental rift system and the concurrent emplacement of an igneous province in Central China (Figure 3). Our study shows that volcanism in South Qinling started from 641 to 637 Ma, whereas volcanism along the northern margin of South China Block occurred from 637 to 635 Ma (Condon et al., 2005). This means that the emplacement of an igneous province in Central China lasted for 6 Myr (641–635 Ma). Because the amount of CO_2 released from a magmatic event in an extensional tectonic setting fluctuates as a function of its size and duration (Tamburello et al., 2018), we considered CO_2 emissions varying from 63,600 to 494,400 Gt over 6 Myr (Supporting Information). According to these constraints, whatever rate of solid Earth degassing is considered (deg0.38 or more), volcanism-related CO_2 emission in the South Qinling
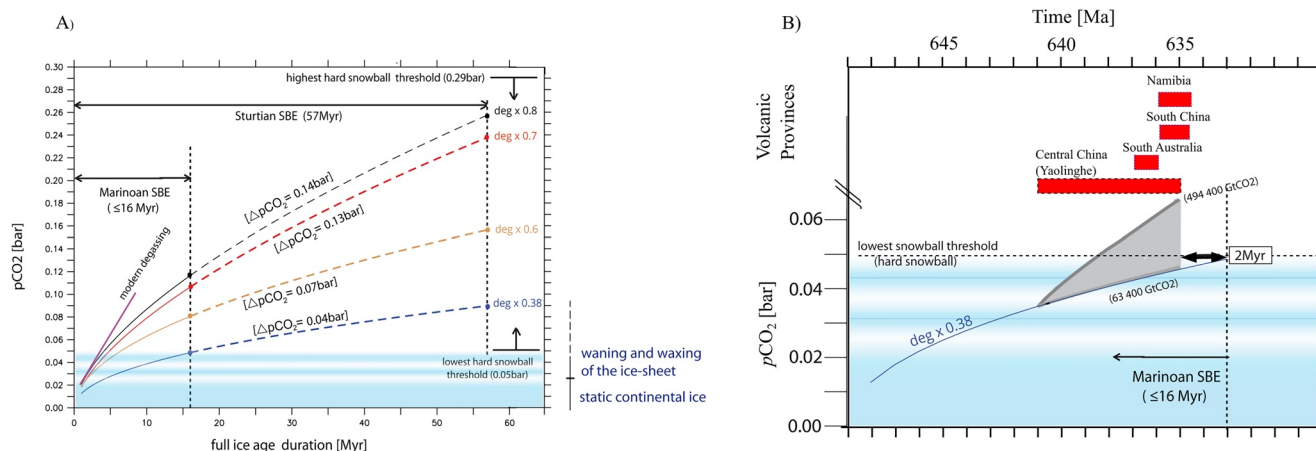
Figure 3. pCO_2 simulated by a biogeochemical model (GEOCLIM) forced by a climate model coupled with an ice-sheet model (Benn et al., 2015) (a) Temporal pCO_2 evolution with different background degassing rates in the context of a hard snowball Earth. Dashed lines represent the amount of carbon between short and long snowball events. Melting thresholds for short and long snowball events are based on their duration (16 and 57 Myr, respectively), all being encompassed within thresholds estimated by climate models from 0.29 (Pierrehumbert, 2004) to 0.05 bars (Benn et al., 2015) assuming a white surface (snow and ice). Melting thresholds for a mudball earth (Abbot & Pierrehumbert, 2010) can be estimated to be at least 1/3 of a clean snowball earth (i.e., 0.1 instead of 0.29 bar) while de Vrese et al. (2021) suggests lower pCO_2 for initiating melting. Ice-sheet behavior is based on climate-ice-sheet model simulations (Benn et al., 2015). (b) Influence of the Yaolinghe rift system and other volcanic provinces on the snowball Earth duration for deg038 experiment (aerial volcanic flux ~0.38 modern conditions). The emplacement has been integrated over 6 Myr to cover all volcanic provinces. Our simulations show how a speed-up in degassing would have foreshortened the Marinoan snowball Earth by 2–5 Myr (i.e., 11–14 Myr duration instead of 16 Myr) under various volcanic emission intensities (gray band).

rift pales in comparison to the mass of carbon already stored in the atmosphere. As illustrated by the deg0.38 case (Figure 3a), even with 494,400 Gt/6 Myr, the rise of pCO_2 falls short (<0.07 bar) of the CO_2 limit required for the onset of the Sturtian deglaciation (~0.09 bar CO_2). Consequently, except for considering a drastic change in the tectonic regime that increased the degassing rate by a significant amount, a lower glacial melting threshold can be expected for the Marinoan.

We estimated CO_2 thresholds that triggered the Marinoan deglaciation by shifting the ice-age duration from 57 to 16 Myr (Figure 3a). Based on the same set of simulations, deglaciation thresholds ($pCO_{2\ (16\ Myr)}$) change significantly, but remain fully encompassed within melting thresholds estimated by climate models (Figure 3a). With the lowest degassing rate (deg0.38), the melting threshold for the Marinoan (~0.05 bar) should be twice compared to that of the Sturtian (0.09 bar). The discrepancy between the Sturtian/Marinoan thresholds increases with the enhancement of degassing, with the most significant rise falling between deg0.6 (ΔpCO_2~0.07) and deg0.7 (ΔpCO_2~0.13) due to the nonlinear rate of accumulation. By considering the South Qinling rift system and other volcanic provinces, we observe that only a very massive carbon release may shorten the ice age (Figure 3a), regardless of pulsed or continuous degassing (see Supporting Information).

4. Discussion and Conclusions

Herein, we highlight that elevated CO_2 emissions induced by magmatism related to rifting and other volcanic provinces do not directly trigger the meltback, even if abnormally high atmospheric CO_2 concentrations amassed by magmatism during glaciation have facilitated the Earth system to begin its escape from the pan-glacial state. Nonetheless, an indirect deglacial scenario can be ascribed to volcanism-induced dust emission and its effect on planetary albedo.

4.1. Snowball Earth Deglaciation Threshold

During the snowball state, volcanism would reduce the surface albedo by emitting volcanic dust. Rhyolites and tuffaceous breccias of the Yaolinghe Group (Figure S1 in Supporting Information S1) represent major volcanic activity from 641 to 637 Ma (4 Myr) before the termination of the Marinoan ice age when PCO_2 was already high (>0.4 bar) based on simulations. The interplay between the hydrological cycle and high pCO_2 caused slow warming, which would reduce snow albedo (de Vrese et al., 2021) and the accumulation of dusty ice in the

equatorial zone (Pierrehumbert et al., 2011). As the South Qinling rift system and other volcanic provinces predate the termination of the Marinoan by a few million years, they would have led to a major reduction in albedo by volcanic dust accumulation (Abbot & Pierrehumbert, 2010). This transformation is one of the main consequences that lowered the pCO$_2$ threshold for deglaciation by 50% or more (Abbot & Pierrehumbert, 2010; de Vrese et al., 2021). In this context, elevated CO$_2$ in the atmosphere induced by magmatism, if not the sole cause of meltback, must have prompted the planet to escape from its pan-glacial state.

These results thus support a very clean, high-albedo snowball for the Sturtian ice age. Under a regime of an ice-covered white Earth, an intense radiative forcing is required to overcome the cooling effect induced by the highly reflective surface, which means a high pCO$_2$ threshold. A long-lived snowball event (57 Myr) implies a high pCO$_2$ threshold, which contrasts with those inferred from climate simulations incorporating dust-snow/ice interplay. By assuming a weak background degassing through the Cryogenian, CO$_2$ and volcanic dust emissions would be less intense, thus allowing glaciers to develop while the darkening induced by dust should be balanced with cleaning from surface meltwater draining accumulated dust through moulins (Goodman & Strom, 2013). Such a condition may facilitate the existence of a long-lived global ice age where the foreshortening of the Marinoan can be seen as the direct result of the South Qinling rift and its long-lasting volcanic activity. In this context, such additional CO$_2$ emissions may shorten the Marinoan snowball by 2–5 Myr (Figure 3b).

Despite less intense CO$_2$ and volcanic dust emissions, such a scenario is supported by geological evidence. Higher than 0.05 bar pCO$_2$ points to a smaller extent of land ice cover (Figure S10 in Supporting Information S1). Whatever the degassing rate (0.38–0.8), after 57 Myr, the continental ice sheet has already started to melt and potentially vanished completely (Benn et al., 2015). As a result, retreat of equatorial sea ice sheets marking the termination of hard snowball conditions would not be associated with an intense freshwater flux coming from the melting of continental ice sheets. Finally, clumped oxygen isotope analyses of Marinoan cap carbonates also suggest low pCO$_2$ (<0.08 bar) even if this estimation does not necessarily represent the maximum pCO$_2$ level (H. Bao et al., 2009). Nevertheless, according to our simulations highlighting highly reduced continental weathering (Figure S13 in Supporting Information S1), the syn-sedimentary dolomite precipitation remains a conundrum (Hood et al., 2021). If the alkalinity is carried by the dissolution of deep sea carbonates (Le Hir, Goddéris, et al., 2008), a major part of the ocean should be undersaturated and characterized by a low Mg/Ca ratio (assuming that calcite is the dominant dissolved carbonate), a process inhibiting dolomite formation.

4.2. Comparison of Yaolinghe and Other Magmatic Emissions Through the Cryogenian

"Fire and ice" causal relationships have been suggested previously for Cryogenian climate fluctuations. The initiation of the Sturtian is suggested to have been induced by weathering of basalts and/or the injection of sulfate aerosols into the stratosphere during the low-latitude eruption of a large igneous province related to Rodinia breakup (Cox et al., 2016; Goddéris et al., 2003; Macdonald & Wordsworth, 2017). Termination of the Sturtian may have been induced by volcanic CO$_2$ emissions (Hoffman et al., 2017; Zhou et al., 2019). Likewise, magmatism-related termination of the Marinoan glaciation is also suggested in the current work. In particular, the Yaolinghe rift-related magmatism likely played a pivotal role due to its long-lasting volcanic activity.

In addition to the Yaolinghe magmatism, the end of the Marinoan also experienced active rift-related volcanism in the Australia, Tarim, Siberia, and Congo cratons with an age range of ca. 643–635 Ma (Calver et al., 2013; Condon et al., 2005; Prave et al., 2016; Vernikovsky et al., 1999; Yarmolyuk et al., 2005; Zhu et al., 2008). Within uncertainties, these magmatic events were all synchronous with end-Marinoan magmatism in South Qinling and the northern margin of the Yangtze block (L. J. Wang, Griffin, et al., 2013; M. Wang, Wang, & Sun, 2013; M. X. Wang, Wang, & Zhao, 2013). Of these, successive emplacement of volcanic provinces approaching deglaciation occurred in South Australia (636.4 ± 0.45 Ma; Calver et al., 2013), then South China (635.2 ± 0.57 Ma; Condon et al., 2005), and Namibia (635.2 ± 0.59 Ma; Prave et al., 2016), where these coordinated rift-related volcanic provinces are associated with final stages of the breakup of supercontinent Rodinia (Gernon et al., 2016; Mitchell et al., 2019). Considering uncertainties for CO$_2$ and dust emissions, multiple volcanic sources may be considered as a likely scenario with a dominant source coming from the South Qinling region. The apparent discrepancy between the end of glaciation (635 Ma) and the prolonged magmatic activity (641–637 Ma) highlights the importance of cumulative effect of CO$_2$ and dust emissions.

No thick volcanic sequences have been found near the terminal Sturtian interval, even though finding such an occurrence—if one existed—would be a much sought-after geochronological constraint on the timing of deglaciation. Unlike the Marinoan glaciation, the purported terminal Sturtian glaciation tuffs do not appear to be associated with any thick volcanic sequences and their occurrences are restricted to South China and South Australia (Cox et al., 2018; Fanning & Link, 2008; Liu et al., 2015; S. Zhang et al., 2008; Zhou et al., 2004, 2019). In South China, two zircon SIMS U-Pb ages on tuffs of 654.5 ± 3.8 Ma and 654.2 ± 2.7 Ma were reported from interglacial successions (Liu et al., 2015; S. Zhang et al., 2008), and one zircon SIMS U-Pb age on a tuff of 662.9 ± 4.3 Ma was documented from within a Sturtian cap carbonate (Zhou et al., 2004). The latter age was refined to 658.8 ± 0.5 Ma using high-precision TIMS U-Pb dating (Zhou et al., 2019). In South Australia, a zircon SIMS U-Pb age of 659.7 ± 5.3 Ma and a zircon TIMS U-Pb age of 663.03 ± 0.11 Ma were reported from tuffs from the top of the Sturtian glaciogenic diamictite (Cox et al., 2018; Fanning & Link, 2008). None of these tuffs are associated, however, with known synchronous volcanism.

In contrast, both tuffs and synchronous large piles of volcanic rocks with ages spanning several pulses from 700 to 670 Ma are reported not close to deglaciation, but during the Sturtian glaciation (Balgord et al., 2013; Fanning & Link, 2008; Ferri et al., 1999; Goodge et al., 2002; Lan, Li, Zhang, & Li, 2015; Lan, Li, Zhu, et al., 2015; Lund et al., 2003, 2010). Specifically, volcaniclastic rocks are reported from the middle Sturtian glaciogenic diamictite in northern Utah, along the North American Cordilleran margin that yields a SIMS U-Pb age of 703 ± 6 Ma (Balgord et al., 2013). A thick sequence of volcanic rocks with indistinguishable zircon SIMS U-Pb ages of 685 ± 7 Ma and 684 ± 4 Ma occurs in the middle of the Sturtian glaciogenic diamictite in Central Idado, USA (Lund et al., 2003, 2010). Synchronous volcanic tuffs are also reported from the middle Sturtian glaciogenic diamictites in Idaho (Fanning & Link, 2008) as well as in South China (Lan, Li, Zhang, & Li, 2015; Lan, Li, Zhu, et al., 2015), with zircon SIMS U-Pb ages of 686 ± 4 Ma and 691 ± 12 Ma, respectively. Volcanic rocks are reported from a purported Sturtian glaciogenic diamictite in Yukon, Canada (Ferri et al., 1999) and Antarctica (Goodge et al., 2002) with zircon TIMS U-Pb ages of 688.6 + 9.5/−6.2 Ma and 667.8 ± 0.6 Ma, respectively. Synchronous volcanic tuffs from the top Sturtian glaciogenic diamictite in Idaho, Western USA gave a zircon SIMS U-Pb age of 667 ± 2 Ma (Fanning & Link, 2008), whereas synchronous volcaniclastic rocks from the middle Sturtian glaciogenic diamictite in northern Utah give a SIMS U-Pb age of 667 ± 5 Ma (Balgord et al., 2013). Overall, these volcanic activities are temporally spread out and predate the termination of the Sturtian by 10–30 Myr. Thus, the Marinoan glaciation was foreshortened by a major and temporally focused pulse of volcanism that the Sturtian glaciation did not experience and therefore took longer to accumulate the requisite CO_2 levels for deglaciation. That is, the lack of volcanism near the end of the Sturtian is the main reason for its longer duration compared to the Marinoan.

Data Availability Statement

All data from this study are available in the online content of this paper and from the Open Science Framework (https://osf.io/qcdtw/?view_only=73f869b59b2b4660a6b5af6f320c3d23).

References

Abbot, D. S., & Pierrehumbert, R. T. (2010). Mudball: Surface dust and snowball Earth deglaciation. *Journal of Geophysical Research*, *115*(D3), D03104. https://doi.org/10.1029/2009JD012007

Abbot, D. S., Voigt, A., Branson, M., Pierrehumbert, R., Pollard, D., Le Hir, G., & Koll, D. (2012). Clouds and snowball Earth deglaciation. *Geophysical Research Letters*, *39*. https://doi.org/10.1029/2012GL052861

Balgord, E. A., Yonkee, W. A., Link, P. K., & Fanning, C. M. (2013). Stratigraphic, geochronologic, and geochemical record of the Cryogenian Perry Canyon Formation, northern Utah: Implications for Rodinia rifting and snowball Earth glaciation. *The Geological Society of America Bulletin*, *125*(9–10), 1442–1467. https://doi.org/10.1130/B30860.1

Bao, H., Fairchild, I. J., Wynn, P. M., & Spotl, C. (2009). Stretching the envelope of past surface environments: Neoproterozoic glacial lakes from Svalbard. *Science*, *323*(5910), 119–122. https://doi.org/10.1126/science.1165373

Bao, X., Zhang, S., Jiang, G., Wu, H., Li, H., Wang, X., et al. (2018). Cyclostratigraphic constraints on the duration of the Datangpo formation and the onset age of the Nantuo (Marinoan) glaciation in South China. *Earth and Planetary Science Letters*, *483*, 52–63. https://doi.org/10.1016/j.epsl.2017.12.001

Benn, D. I., Le Hir, G., Bao, H., Donnadieu, Y., Dumas, C., Fleming, E. J., et al. (2015). Orbitally forced ice sheet fluctuations during the Marinoan Snowball Earth glaciation. *Nature Geoscience*, *8*(9), 704–707. https://doi.org/10.1038/ngeo2502

Cai, Z., Xiong, X., Luo, H., Wu, D., Sun, S., Yao, B., & Wang, S. (2007). Forming age of the volcanic rocks of the Yaolinghe group from Wudang block, southern Qinling mountain: Constraint from grain-zircon U-Pb dating. *Acta Geologica Sinica*, *81*, 620–625.

Calver, C. R., Crowley, J. L., Wingate, M. T. D., Evans, D. A. D., Raub, T. D., & Schmitz, M. D. (2013). Globally synchronous Marinoan deglaciation indicated by U-Pb geochronology of the Cottons Breccia, Tasmania, Australia. *Geology*, *41*(10), 1127–1130. https://doi.org/10.1130/G34568.1

Condon, D., Zhu, M., Bowring, S., Wang, W., Yang, A., & Jin, Y. (2005). U-Pb ages from the Neoproterozoic Doushantuo Formation, China. *Science*, *308*(5718), 95–98. https://doi.org/10.1126/science.1107765

Cox, G. M., Halverson, G. P., Stevenson, R. K., Vokaty, M., Poirier, A., Kunzmann, M., et al. (2016). Continental flood basalt weathering as a trigger for Neoproterozoic Snowball Earth. *Earth and Planetary Science Letters*, *446*, 89–99. https://doi.org/10.1016/j.epsl.2016.04.016

Cox, G. M., Isakson, V., Hoffman, P. F., Gernon, T. M., Schmitz, M. D., Shahin, S., et al. (2018). South Australian U-Pb zircon (CA-ID-TIMS) age supports globally synchronous Sturtian deglaciation. *Precambrian Research*, *315*, 257–263. https://doi.org/10.1016/j.precamres.2018.07.007

Deng, Q., Yang, Q., Mao, X., & Kong, L. (2016). Study of lithostratigraphic sequences and chronology of middle-late Nanhua in Wudang-Suizhou area. *Resources Environment & Engineering*, *30*, 132–142.

de Vrese, P., Stacke, T., Caves Rugenstein, J., Goodman, J., & Brovkin, V. (2021). Snowfall-albedo feedbacks could have led to deglaciation of snowball Earth starting from mid-latitudes. *Communications Earth & Environment*, *2*(1), 91. https://doi.org/10.1038/s43247-021-00160-4

Dong, Y., Safonova, I., & Wang, T. (2016). Tectonic evolution of the Qinling orogen and adjacent orogenic belts. *Gondwana Research*, *30*, 1–5. https://doi.org/10.1016/j.gr.2015.12.001

Donnadieu, Y., Pierrehumbert, R., Jacob, R., & Fluteau, F. (2006). Modelling the primary control of paleogeography on Cretaceous climate. *Earth and Planetary Science Letters*, *248*(1–2), 426–437. https://doi.org/10.1016/j.epsl.2006.06.007

Erwin, D. H., Laflamme, M., Tweedt, S. M., Sperling, E. A., Pisani, D., & Peterson, K. J. (2011). The Cambrian conundrum: Early divergence and later ecological success in the early history of animals. *Science*, *334*(6059), 1091–1097. https://doi.org/10.1126/science.1206375

Fanning, C. M., & Link, P. K. (2008). Age constraints for the Sturtian glaciation: Data from the Adelaide geosyncline, south Australia and pocatello formation, Idaho, USA. In *Geological Society of Australia Abstracts, 91, Selwyn Symposium 2008, Mel-Bourne* (pp. 57–62).

Ferri, F., Rees, C. J., Nelson, J. L., & Legun, A. S. (1999). Geology and mineral deposits of the northern Kechika trough between Gataga River and the 60th parallel. *Bulletin of British Columbia Ministry of Energy and Mines*, *107*, 1–122.

Gernon, T. M., Hincks, T. K., Tyrrell, T., Rohling, E. J., & Palmer, M. R. (2016). Snowball Earth ocean chemistry driven by extensive ridge volcanism during Rodinia breakup. *Nature Geoscience*, *9*(3), 242–248. https://doi.org/10.1038/ngeo2632

Goddéris, Y., Donnadieu, Y., Nédélec, A., Dupré, B., Dessert, C., Grard, A., et al. (2003). The sturtian 'snowball' glaciation: Fire and ice. *Earth and Planetary Science Letters*, *211*(1–2), 1–12. https://doi.org/10.1016/S0012-821X(03)00197-3

Goodge, J. W., Myrow, P., Williams, I. S., & Bowring, S. A. (2002). Age and provenance of the Beardmore group, Antarctica: Constraints on Rodinia supercontinent breakup. *The Journal of Geology*, *110*(4), 393–406. https://doi.org/10.1086/340629

Goodman, J. C., & Strom, D. C. (2013). Feedbacks in a coupled ice-atmosphere-dust model of the glacial Neoproterozoic "Mudball Earth". *Journal of Geophysical Research: Atmospheres*, *118*(20), 11546–11557. https://doi.org/10.1002/jgrd.50849

Harland, W. B., & Rudwick, M. J. S. (1964). The great infra-Cambrian ice age. *Scientific American*, *211*(2), 28–36. https://doi.org/10.1038/scientificamerican0864-28

Hoffman, P. F., Abbot, D. S., Ashkenazy, Y., Benn, D. I., Brocks, J. J., Cohen, P. A., et al. (2017). Snowball Earth climate dynamics and Cryogenian geology-geobiology. *Science Advances*, *3*(11), e1600983. https://doi.org/10.1126/sciadv.1600983

Hoffman, P. F., Kaufman, A. J., Halverson, G. P., & Schrag, D. P. (1998). A Neoproterozoic snowball earth. *Science*, *281*(5381), 1342–1346. https://doi.org/10.1126/science.281.5381.1342

Hoffman, P. F., & Schrag, D. P. (2002). The snowball Earth hypothesis: Testing the limits of global change. *Terra Nova*, *14*(3), 129–155. https://doi.org/10.1046/j.1365-3121.2002.00408.x

Hood, A. V. S., Penman, D. E., Lechte, M. A., Wallace, M. W., Giddings, J. A., & Planavsky, N. J. (2021). Neoproterozoic syn-glacial carbonate precipitation and implications for a snowball Earth. *Geobiology*, 1–19. https://doi.org/10.1111/gbi.12470

Kirschvink, J. L. (1992). Late proterozoic low-latitude global glaciation: The snowball Earth. In *The proterozoic biosphere* (pp. 51–52). Cambridge University Press.

Lan, Z., Li, X., Zhu, M., Chen, Z.-Q., Zhang, Q., Li, Q., et al. (2014). A rapid and synchronous initiation of the wide spread Cryogenian glaciations. *Precambrian Research*, *255*, 401–411. https://doi.org/10.1016/j.precamres.2014.10.015

Lan, Z., Li, X.-H., Zhang, Q., & Li, Q.-L. (2015). Global synchronous initiation of the 2nd episode of Sturtian glaciation: SIMS zircon U–Pb and O isotope evidence from the Jiangkou group, south China. *Precambrian Research*, *267*, 28–38. https://doi.org/10.1016/j.precamres.2015.06.002

Lan, Z., Li, X.-H., Zhu, M., Zhang, Q., & Li, Q.-L. (2015). Revisiting the Liantuo Formation in Yangtze block, south China: SIMS U–Pb zircon age constraints and regional and global significance. *Precambrian Research*, *263*, 123–141. https://doi.org/10.1016/j.precamres.2015.03.012

Le Hir, G., Donnadieu, Y., Krinner, G., & Ramstein, G. (2010). Toward the snowball Earth deglaciation. *Climate Dynamics*, *35*(2–3), 285–297. https://doi.org/10.1007/s00382-010-0748-8

Le Hir, G., Goddris, Y., Donnadieu, Y., & Ramstein, G. A. (2008). Geochemical modeling study of the evolution of the chemical composition of seawater linked to a "snowball" glaciation. *Biogeosciences*, *5*(1), 253–267. https://doi.org/10.5194/bg-5-253-2008

Le Hir, G., Ramstein, G., Donnadieu, Y., & Goddéris, Y. (2008). Scenario for the evolution of atmospheric pCO2 during a snowball Earth. *Geology*, *36*(1), 47. https://doi.org/10.1130/G24124A.1

Li, X., Li, Z.-X., Zhou, H., Liu, Y., & Kinny, P. D. (2002). U–Pb zircon geochronology, geochemistry and Nd isotopic study of Neoproterozoic bimodal volcanic rocks in the Kangdian Rift of South China: Implications for the initial rifting of Rodinia. *Precambrian Research*, *113*(1–2), 135–154. https://doi.org/10.1016/S0301-9268(01)00207-8

Ling, W., Ren, B., Duan, R., Liu, X., Mao, X., Peng, L., et al. (2008). Timing of the Wudangshan, Yaolinghe volcanic sequences and mafic sills in South Qinling: U–Pb zircon geochronology and tectonic implication. *Chinese Science Bulletin*(53), 2192–2199. https://doi.org/10.1007/s11434-008-0269-6

Ling, W. L., Duan, R., Liu, X., Cheng, J., Mao, X., Peng, L., et al. (2010). U-Pb dating of detrital zircons from the Wudangshan Group in the South Qinling and its geological significance. *Chinese Science Bulletin*, *55*(22), 2440–2448. https://doi.org/10.1007/s11434-010-3095-6

Liu, P., Li, X., Chen, S., Lan, Z., Yang, B., Shang, X., & Yin, C. (2015). New SIMS U–Pb zircon age and its constraint on the beginning of the Nantuo glaciation. *Science Bulletin*, *60*(10), 958–963. https://doi.org/10.1007/s11434-015-0790-3

Lund, K., Aleinikoff, J. N., Evans, K. V., duBray, E. A., Dewitt, E. H., & Unruh, D. M. (2010). SHRIMP U-Pb dating of recurrent Cryogenian and Late Cambrian-Early Ordovician alkalic magmatism in central Idaho: Implications for Rodinian rift tectonics. *The Geological Society of America Bulletin*, *122*(3–4), 430–453. https://doi.org/10.1130/B26565.1

Lund, K., Aleinikoff, J. N., Evans, K. V., & Fanning, C. M. (2003). SHRIMP U-Pb geochronology of Neoproterozoic Windermere Supergroup, central Idaho: Implications for rifting of Western Laurentia and synchroneity of Sturtian glacial deposits. *The Geological Society of America Bulletin*, *115*, 349–372. https://doi.org/10.1130/0016-7606(2003)115<0349:SUPGON>2.0.CO;2

Macdonald, F. A., & Wordsworth, R. (2017). Initiation of snowball Earth with volcanic sulfur aerosol emissions. *Geophysical Research Letters*, *44*, 1938–1946. https://doi.org/10.1002/2016GL072335

Mills, B. J. W., Scotese, C. R., Walding, N. G., Shields, G. A., & Lenton, T. M. (2017). Elevated CO_2 degassing rates prevented the return of Snowball Earth during the Phanerozoic. *Nature Communications*, *8*(1), 1110. https://doi.org/10.1038/s41467-017-01456-w

Mitchell, R. N., Gernon, T. M., Nordsvan, A., Cox, G. M., Li, Z., & Hoffman, P. F. (2019). *Hit or miss: Glacial incisions of snowball Earth* (pp. 381–389). Terra Nova. https://doi.org/10.1111/ter.12400

Nelson, L. L., Smith, E. F., Hodgin, E. B., Crowley, J. L., Schmitz, M. D., & Macdonald, F. A. (2020). Geochronological constraints on Neoproterozoic rifting and onset of the Marinoan glaciation from the Kingston peak formation in Death valley, California (USA). *Geology*, *48*(11), 1083–1087. https://doi.org/10.1130/G47668.1

Pierrehumbert, R. T. (2004). High levels of atmospheric carbon dioxide necessary for the termination of global glaciation. *Nature*, *429*(6992), 646–649. https://doi.org/10.1038/nature02640

Pierrehumbert, R. T. (2005). Climate dynamics of a hard snowball Earth. *Journal of Geophysical Research*, *110*(D1), D01111. https://doi.org/10.1029/2004JD005162

Pierrehumbert, R. T., Abbot, D. S., Voigt, A., & Koll, D. (2011). Climate of the Neoproterozoic. *Annual Review of Earth and Planetary Sciences*, *39*(1), 417–460. https://doi.org/10.1146/annurev-earth-040809-152447

Prave, A. R., Condon, D. J., Hoffmann, K. H., Tapster, S., & Fallick, A. E. (2016). Duration and nature of the end-Cryogenian (Marinoan) glaciation. *Geology*, *44*(8), 631–634. https://doi.org/10.1130/G38089.1

Tamburello, G., Pondrelli, S., Chiodini, G., & Rouwet, D. (2018). Global-scale control of extensional tectonics on CO2 Earth degassing. *Nature Communications*, *9*(1), 4608. https://doi.org/10.1038/s41467-018-07087-z

Vernikovsky, V. A., Vernikovskaya, A. E., Sal'nikova, E. B., Kotov, A. B., Chernykh, A. I., Kovach, V. P., et al. (1999). New U–Pb data on the formation of the Predivinsk paleoisland-arc complex (Yenisey Ridge). *Russian Geology and Geophysics*, *40*, 255–259.

Villa, I. M., Bonardi, M. L., De Bièvre, P., Holden, N. E., & Renne, P. R. (2016). IUPAC-IUGS status report on the half-lives of 238U, 235U and 234U. *Geochimica et Cosmochimica Acta*, *172*, 387–392. https://doi.org/10.1016/j.gca.2015.10.011

Wang, J., & Li, Z. (2003). History of Neoproterozoic rift basins in South China: Implications for Rodinia break-up. *Precambrian Research*, *122*(1–4), 141–158. https://doi.org/10.1016/S0301-9268(02)00209-7

Wang, L.-J., Griffin, W. L., Yu, J.-H., & O'Reilly, S. Y. (2013). U–Pb and Lu–Hf isotopes in detrital zircon from Neoproterozoic sedimentary rocks in the northern Yangtze Block: Implications for Precambrian crustal evolution. *Gondwana Research*, *23*(4), 1261–1272. https://doi.org/10.1016/j.gr.2012.04.013

Wang, M., Wang, C. Y., & Sun, Y. (2013). Mantle source, magma differentiation and sulfide saturation of the ∼637Ma Zhouan mafic–ultramafic intrusion in the northern margin of the Yangtze Block, Central China. *Precambrian Research*, *228*, 206–222. https://doi.org/10.1016/j.precamres.2013.01.015

Wang, M. X., Wang, C., & Zhao, J. (2013). Zircon U/Pb dating and Hf-O isotopes of the Zhouan ultramafic intrusion in the northern margin of the Yangtze Block, SW China: Constraints on the nature of mantle source and timing of the supercontinent Rodinia breakup. *Chinese Science Bulletin*, *58*(7), 777–787. https://doi.org/10.1007/s11434-012-5435-1

Wang, R., Xu, Z., Santosh, M., Yao, Y., Gao, L., & Liu, C. (2016). Late Neoproterozoic magmatism in South Qinling, central China: Geochemistry, zircon U-Pb-Lu-Hf isotopes and tectonic implications. *Tectonophysics*, *683*, 43–61. https://doi.org/10.1016/j.tecto.2016.05.050

Xue, H. M., Ma, F., & Song, Y. Q. (2011). Geochemistry and SHRIMP zircon U–Pb data of Neoproterozoic metamorphic magmatism rocks in the Suizhou-Zaoyang area, northern margin of the Yangtze Craton, Central China. *Acta Petrologica Sinica*, *27*, 1116–1130.

Yarmolyuk, V. V., Kovalenko, V. I., Sal'nikova, E. B., Nikiforov, A. V., Kotov, A. B., & Vladykin, N. V. (2005). Late Riphean rifting and breakup of laurasia: Data on geochronological studies of ultramafic alkaline complexes in the southern framing of the Siberian craton. *Doklady Earth Sciences*, *404*, 1031–1036.

Zhang, R., Sun, Y., Zhang, X., Ao, W., & Santosh, M. (2016). Neoproterozoic magmatic events in the south Qinling belt, China: Implications for amalgamation and breakup of the Rodinia supercontinent. *Gondwana Research*, *30*, 6–23. https://doi.org/10.1016/j.gr.2015.06.015

Zhang, S., Jiang, G., & Han, Y. (2008). The age of the Nantuo formation and Nantuo glaciation in South China. *Terra Nova*, *20*(4), 289–294. https://doi.org/10.1111/j.1365-3121.2008.00819.x

Zhou, C., Huyskens, M. H., Lang, X., Xiao, S., & Yin, Q.-Z. (2019). Calibrating the terminations of Cryogenian global glaciations. *Geology*, *47*(3), 251–254. https://doi.org/10.1130/G45719.1

Zhou, C., Tucker, R., Xiao, S., Peng, Z., Yuan, X., & Chen, Z. (2004). New constraints on the ages of Neoproterozoic glaciations in south China. *Geology*, *32*(5), 437. https://doi.org/10.1130/G20286.1

Zhu, X., Chen, F., Liu, B., Zhang, H., & Zhai, M. (2015). Geochemistry and zircon ages of mafic dikes in the south Qinling, central China: Evidence for late Neoproterozoic continental rifting in the northern Yangtze block. *International Journal of Earth Sciences*, *104*(1), 27–44. https://doi.org/10.1007/s00531-014-1056-z

Zhu, X., Chen, F., Nie, H., Siebel, W., Yang, Y., Xue, Y., & Zhai, M. (2014). Neoproterozoic tectonic evolution of South Qinling, China: Evidence from zircon ages and geochemistry of the Yaolinghe volcanic rocks. *Precambrian Research*, *245*, 115–130. https://doi.org/10.1016/j.precamres.2014.02.005

Zhu, X., Chen, F., Wang, F., Pham, T. H., Wang, F., & Zhang, F. (2008). Zircon U–Pb ages of volcanic and sedimentary rocks of the Wudang Group in the Qinling orogenic belt within Western Henan Province. *Acta Geoscientica Sinica*, *29*, 817–829.

References From the Supporting Information

Ashkenazy, Y., Losch, M., Gildor, H., Mirzayof, D., & Tziperman, E. (2013). Multiple sea-ice states and abrupt MOC transitions in a general circulation ocean model. *Climate Dynamics*, *40*(7–8), 1803–1817. https://doi.org/10.1007/s00382-012-1546-2

Bao, H. M., Fairchild, I. J., Wynn, P. M., & Spotl, C. (2009). Stretching the envelope of past surface environments: Neoproterozoic glacial lakes from Svalbard. *Science*, *323*(5910), 119–122. https://doi.org/10.1126/science.1165373

Barnes, S.-J., Naldrett, A. J., & Gorton, M. P. (1985). The origin of the fractionation of platinum-group elements in terrestrial magmas. *Chemical Geology*, *53*(3–4), 303–323. https://doi.org/10.1016/0009-2541(85)90076-2

Beswick, A. E. (1982). Some geochemical aspects of alteration and genetic relations in komatiitic suites. In *Komatiites* (pp. 283–308). George Allen and Unwin, London.

Black, L. P., Kamo, S. L., Allen, C. M., Davis, D. W., Aleinikoff, J. N., Valley, J. W., et al. (2004). Improved 206Pb/238U microprobe geochronology by the monitoring of a trace-element-related matrix effect; SHRIMP, ID–TIMS, ELA–ICP–MS and oxygen isotope documentation for a series of zircon standards. *Chemical Geology*, *205*(1–2), 115–140. https://doi.org/10.1016/j.chemgeo.2004.01.003

Brune, S., Williams, S. E., & Müller, R. D. (2017). Potential links between continental rifting, CO_2 degassing and climate change through time. *Nature Geoscience*, *10*(12), 941–946. https://doi.org/10.1038/s41561-017-0003-6

Charnay, B., Le Hir, G., Fluteau, F., Forget, F., & Catling, D. C. (2017). A warm or a cold early Earth? New insights from a 3-D climate-carbon model. *Earth and Planetary Science Letters*, *474*, 97–109. https://doi.org/10.1016/j.epsl.2017.06.029

Eby, G. N. (1992). Chemical subdivision of the A-type granitoids: Petrogenetic and tectonic implications. *Geology*, *20*, 641–644.

Foley, S. F., & Fischer, T. P. (2017). An essential role for continental rifts and lithosphere in the deep carbon cycle. *Nature Geoscience*, *10*(12), 897–902. https://doi.org/10.1038/s41561-017-0002-7

Ganino, C., & Arndt, N. T. (2009). Climate changes caused by degassing of sediments during the emplacement of large igneous provinces. *Geology*, *37*(4), 323–326. https://doi.org/10.1130/G25325A.1

Hiess, J., Condon, D. J., McLean, N., & Noble, S. R. (2012). 238U/235U systematics in terrestrial uranium-bearing minerals. *Science*, *335*(6076), 1610–1614. https://doi.org/10.1126/science.1215507

Hu, F., Liu, S., Santosh, M., Deng, Z., Wang, W., Zhang, W., & Yan, M. (2016). Chronology and tectonic implications of Neoproterozoic blocks in the south Qinling orogenic belt, central China. *Gondwana Research*, *30*, 24–47. https://doi.org/10.1016/j.gr.2015.01.006

Hunt, J. A., Zafu, A., Mather, T. A., Pyle, D. M., & Barry, P. H. (2017). Spatially variable CO_2 degassing in the Main Ethiopian Rift: Implications for magma storage, volatile transport and rift-related emissions. *Geochemistry, Geophysics, Geosystems*, *18*(10), 3714–3737. https://doi.org/10.1002/2017GC006975

Huyskens, M. H., Iizuka, T., & Amelin, Y. (2012). Evaluation of colloidal silicagels for lead isotopic measurements using thermal ionisation mass spectrometry. *Journal of Analytical Atomic Spectrometry*, *27*(9), 1439. https://doi.org/10.1039/c2ja30083d

Huyskens, M. H., Zink, S., & Amelin, Y. (2016). Evaluation of temperature-time conditions for the chemical abrasion treatment of single zircons for U–Pb geochronology. *Chemical Geology*, *438*, 25–35. https://doi.org/10.1016/j.chemgeo.2016.05.013

Hyde, W. T., Crowley, T. J., Baum, S. K., & Peltier, W. R. (2000). Neoproterozoic 'snowball Earth' simulations with a coupled climate/ice-sheet model. *Nature*, *405*(6785), 425–429. https://doi.org/10.1038/35013005

Jaffey, A. H., Flynn, K. F., Glendenin, L. E., Bentley, W. C., & Essling, A. M. (1971). Precision measurement of half-lives and specific activities of U 235 and U 238. *Physical Review C*, *4*(5), 1889–1906. https://doi.org/10.1103/PhysRevC.4.1889

Klaver, M., Smeets, R. J., Koornneef, J. M., Davies, G. R., & Vroon, P. Z. (2016). Pb isotope analysis of ng size samples by TIMS equipped with a 10 ^{13} Ω resistor using a ^{207}Pb–^{204}Pb double spike. *Journal of Analytical Atomic Spectrometry*, *31*(1), 171–178. https://doi.org/10.1039/C5JA00130G

Krogh, T. E. (1973). A low-contamination method for hydrothermal decomposition of zircon and extraction of U and Pb for isotopic age determinations. *Geochimica et Cosmochimica Acta*, *37*(3), 485–494. https://doi.org/10.1016/0016-7037(73)90213-5

Le Hir, G., Ramstein, G., Donnadieu, Y., & Goddéris, Y. (2008). Scenario for the evolution of atmospheric pCO$_2$ during a snowball Earth. *Geology*, *36*(1), 47. https://doi.org/10.1130/G24124A.1

Li, C.-F., Wang, X.-C., Guo, J.-H., Chu, Z.-Y., & Feng, L.-J. (2016). Rapid separation scheme of Sr, Nd, Pb, and Hf from a single rock digest using a tandem chromatography column prior to isotope ratio measurements by mass spectrometry. *Journal of Analytical Atomic Spectrometry*, *31*(5), 1150–1159. https://doi.org/10.1039/C5JA00477B

Li, C.-F., Wu, H.-Q., Chu, Z.-Y., Wang, X.-C., Li, Y.-L., & Guo, J.-H. (2019). Precise determination of radiogenic Sr and Nd isotopic ratios and Rb, Sr, Sm, Nd elemental concentrations in four coal ash and coal fly ash reference materials using isotope dilution thermal ionization mass spectrometry. *Microchemical Journal*, *146*, 906–913. https://doi.org/10.1016/j.microc.2019.02.034

Li, X. H., Li, Z.-X., Zhou, H., Liu, Y., & Kinny, P. D. (2002). U–Pb zircon geochronology, geochemistry and Nd isotopic study of Neoproterozoic bimodal volcanic rocks in the Kangdian Rift of South China: Implications for the initial rifting of Rodinia. *Precambrian Research*, *113*(1–2), 135–154. https://doi.org/10.1016/S0301-9268(01)00207-8

Ludwig, K. (2012). *A geochronological toolkit for Microsoft Excel* (Vol. 1–5). Berkeley Geochronology Center, Special Publication.

Lugmair, G., & Carlson, R. (1978). The Sm-Nd history of KREEP. *Lunar and Planetary Science Conference Proceedings*, 689–704.

Meschede, M. (1986). A method of discriminating between different types of mid-ocean ridge basalts and continental tholeiites with the Nb-Zr-Y diagram. *Chemical Geology*, *56*(3–4), 207–218. https://doi.org/10.1016/0009-2541(86)90004-5

Mussard, M., Le Hir, G., Fluteau, F., Lefebvre, V., & Goddéris, Y. (2014). Modeling the carbon-sulfate interplays in climate changes related to the emplacement of continental flood basalts. In G. Keller, & A. C. Kerr (Eds.), *Volcanism, impacts, and mass extinctions: Causes and effects*. Geological Society of America. https://doi.org/10.1130/2014.2505(17

Richter, S., Eykens, R., Kühn, H., Aregbe, Y., Verbruggen, A., & Weyer, S. (2010). New average values for the n(^{238}U)/n(^{235}U) isotope ratios of natural uranium standards. *International Journal of Mass Spectrometry*, *295*(1–2), 94–97. https://doi.org/10.1016/j.ijms.2010.06.004

Schaller, M. F., Wright, J. D., & Kent, D. V. (2011). Atmospheric PCO2 perturbations associated with the central Atlantic magmatic province. *Science*(331), 1404–1408.

Schmitz, M. D., & Schoene, B. (2007). Derivation of isotope ratios, errors, and error correlations for U-Pb geochronology using ^{205}Pb-^{235}U -(^{233}U)-spiked isotope dilution thermal ionization mass spectrometric data. *Geochemistry, Geophysics, Geosystems*, *8*(8). https://doi.org/10.1029/2006GC001492

Sun, S. S., & McDonough, W. F. (1989). Chemical and isotopic systematics of oceanic basalts: Implications for mantle composition and processes. *Geological Society, London, Special Publications*, *42*(1), 313–345. https://doi.org/10.1144/GSL.SP.1989.042.01.19

Trinquier, A. (2016). Fractionation of oxygen isotopes by thermal ionization mass spectrometry inferred from simultaneous measurement of ^{17}O/^{16}O and ^{18}O/^{16}O ratios and implications for the ^{182}Hf–^{182}W systematics. *Analytical Chemistry*, *88*(11), 5600–5604. https://doi.org/10.1021/acs.analchem.6b01101

Verbruggen, A., Bauwens, J., Eykens, R., Kehoe, F., Kühn, H., Jacobsson, U., et al. (2008). *Preparation and certification of IRMM-3636, IRMM-3636a and IRMM-3636b*. OPOCE.

von Quadt, A., Wotzlaw, J.-F., Buret, Y., Large, S., Peytcheva, I., & Trinquier, A. (2016). High-precision zircon U/Pb geochronology by ID-TIMS using new 1013 ohm resistors. *Journal of Analytical Atomic Spectrometry*, *31*, 658–665.

Whalen, J. B., Currie, K. L., & Chappell, B. W. (1987). A-type granites: Geochemical characteristics, discrimination and petrogenesis. *Contribution to Mineralogy and Petrology*, *95*, 407–419.

Winchester, J. A., & Floyd, P. A. (1977). Geochemical discrimination of different magma series and their differentiation products using immobile elements. *Chemical Geology*, *20*, 325–343.